Zhang M, Zeng W, Guo R *et al.* Survey on discrete surface Ricci flow. JOURNAL OF COMPUTER SCIENCE AND TECHNOLOGY 30(3): 598–613 May 2015. DOI 10.1007/s11390-015-1548-8

Survey on Discrete Surface Ricci Flow

Min Zhang[1] (章 敏), Wei Zeng[2] (曾 薇), Ren Guo[3] (郭 韧), Feng Luo[4] (罗 锋), and Xianfeng David Gu[1] (顾险峰), *Member, IEEE*

[1] *Department of Computer Science, State University of New York at Stony Brook, Stony Brook, NY 11794-4400, U.S.A.*

[2] *School of Computing and Information Sciences, Florida International University, Miami, Florida 33199, U.S.A.*

[3] *Department of Mathematics, Oregon State University, Corvallis, OR 97331-4605, U.S.A.*

[4] *Department of Mathematics, Rutgers University, Piscataway, NJ 08854, U.S.A.*

E-mail: mzhang@cs.sunysb.edu; wzeng@cs.fiu.edu; guore@math.oregonstate.edu; luo@math.rutgers.edu gu@cs.sunysb.edu

Received April 10, 2014; revised November 12, 2014.

Abstract Ricci flow deforms the Riemannian metric proportionally to the curvature, such that the curvature evolves according to a nonlinear heat diffusion process, and becomes constant eventually. Ricci flow is a powerful computational tool to design Riemannian metrics by prescribed curvatures. Surface Ricci flow has been generalized to the discrete setting. This work surveys the theory of discrete surface Ricci flow, its computational algorithms, and the applications for surface registration and shape analysis.

Keywords Ricci flow, discrete, Riemannian metric, Ricci energy, uniformization theory

1 Introduction

Ricci flow deforms the Riemannian metric proportionally to the curvature, such that the curvature evolves according to a heat diffusion process and eventually becomes constant everywhere. Ricci flow is a powerful tool in geometric analysis for studying low-dimensional topology. It has been successfully applied for the proofs of Poincaré's conjecture and Thurston's geometrization conjecture. Recently, Ricci flow has started making impacts on practical fields and tackling fundamental engineering problems. This work focuses on the theory and algorithm of discrete surface Ricci flow, and its applications on surface registration and shape analysis.

Ricci flow is the tool to design a Riemannian metric using prescribed Gaussian curvature. Ricci flow deforms the Riemannian metric proportionally to the difference between the target curvature and the current curvature, such that the curvature evolves according to a heat diffusion process, and eventually converges to the target curvature. So far, there is no other alternative to achieve this goal. Designing a metric using curvature is fundamental to solving many problems, surface parameterization is equivalent to finding a flat metric for a surface, and surface matching and registration can be converted to image registration using Ricci flow. By using Ricci flow, NP-hard problems in computational topology can be solved practically.

Surface Ricci flow implies the celebrated surface uniformization theorem. Namely, as shown in Fig.1, any closed metric surface can be conformally mapped to the unit sphere $\mathbb{S}^2$, the Euclidean plane $\mathbb{E}^2$ or hyperbolic plane $\mathbb{H}^2$. Similarly, surfaces with boundaries can be mapped to one of these three canonical spaces with circular holes (the so-called circle domains), as shown in Fig.2.

General Ricci flow is defined on arbitrary dimensional Riemannian manifolds. Surface (2-manifold) Ricci flow has unique characteristics, which are crucial for developing discrete theories and designing computational algorithms. First, surface Ricci flow never blows up, namely, the Gauss curvature during the flow is always bounded. This phenomenon ensures the numerical stability of discrete surface Ricci flow. In contrast, 3-manifold Ricci flow will produce singularities,

Survey

and thus topological surgery is unavoidable. Second, surface Ricci flow is conformal, namely, the deformation of the Riemannian metric preserves angles. This fact greatly simplifies both theoretical arguments and algorithmic designs. General Ricci flow is governed by tensor differential equations, whereas surface Ricci flow is described by scalar differential equations. Third, surface Ricci flow has intuitive geometric interpretations, which directly lead to the design of data structures. A conformal deformation transforms infinitesimal circles to infinitesimal circles. This elucidates the geometric nature of the flow. Finally, Ricci flow is variational, namely, Ricci flow is the negative gradient flow of Ricci energy. Accordingly, discrete surface Ricci flow can be formulated as a convex optimization problem, which has a unique global optimum and can be carried out using the efficient Newton's method.

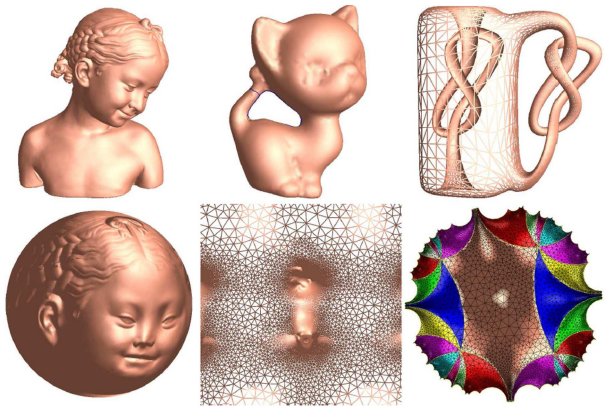

Fig.1. Uniformization for closed surfaces[1].

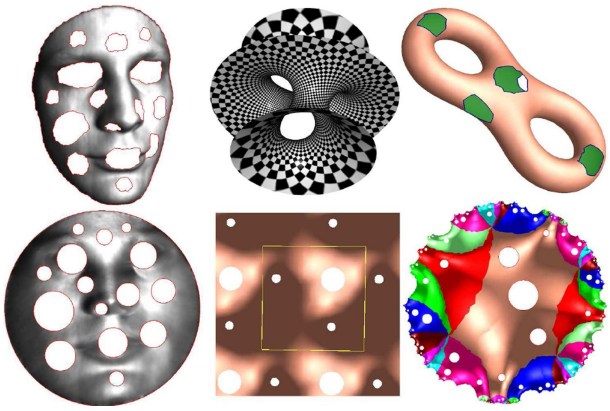

Fig.2. Uniformization for surfaces with boundaries[1].

For the purpose of surface registration and shape analysis, discrete surface Ricci flow has the following unique merits: 1) by Ricci flow, all shapes in real life can be unified to be one of three canonical shapes, the sphere, the plane, or the hyperbolic disk; 2) therefore, most 3-dimensional (3D) geometric problems can be converted to 2-dimensional (2D) image problems, which greatly simplifies the computation; 3) furthermore, this conversion is conformal and preserves the original geometric information; 4) finally, by deforming Riemannian metric, Ricci flow can be used to compute general diffeomorphisms between surfaces.

Ricci flow has demonstrated its great potential by solving various problems in many fields, which can be hardly handled by alternative methods so far. The following are some examples: 1) non-rigid surface registration and tracking in computer vision, 2) global surface parameterization in computer graphics, 3) conformal brain mapping and virtual colonoscopy in medical imaging, 4) the shortest word problem in computational topology, 5) delivery guaranteed greedy routing and load balancing in wireless sensor network, and so on. We believe more and more researchers will realize and appreciate the intrinsic power and beauty of Ricci flow, and more and more fields in engineering and medicine will be impacted by Ricci flow.

2 Groundwork

Ricci flow conformally deforms the Riemannian metrics, such that during the flow, the infinitesimal circles are preserved. This phenomenon inspired Thurston to develop the circle packing method. In his work on constructing hyperbolic metrics on 3-manifolds, Thurston[2] studied a Euclidean (or a hyperbolic) circle packing on a triangulated closed surface with prescribed intersection angles. His work generalizes Andreev's and Koebe's results of circle packing on a sphere[3-5]. Thurston conjectured that the discrete conformal mapping based on circle packing converges to the smooth Riemann mapping when the discrete tessellation becomes finer and finer. Thurston's conjecture has been proved by Rodin and Sullivan[6]. Chow and Luo established the intrinsic connection between circle packing and surface Ricci flow[7].

The rigidity for classical circle packing was proved by Thurston[2], Marden and Rodin[8], Colin de Verdiére[9], Chow and Luo[7], Stephenson[10], and He and Schramm[11]. Bowers and Stephenson[12] introduced inversive distance circle packing which generalizes Andreev-Thurston's intersection angle circle packing. See [10] for more information. Guo gave a proof for local rigidity[13]. Luo studied the combinatorial

Yamabe problem for piecewise flat metrics on triangulated surfaces[14]. Springborn *et al.*[15] considered this combinatorial conformal change of piecewise flat metrics and found an explicit formula of the energy function. Glickenstein[16-17] studied the combinatorial Yamabe flow on 3D piecewise flat manifolds. Recently, Glickenstein[18] set the theory of combinatorial Yamabe flow of piecewise flat metric in a broader context including the theory of circle packing on surfaces. Combinatorial Yamabe flow on hyperbolic surfaces with boundary has been studied by Guo[19]. All the schemes are unified in [20].

The variational approach to circle packing was first introduced by Colin de Verdiére[9]. Since then, many studies on variational principles on circle packing or circle pattern have appeared, for example, studies of Brägger[21], Rivin[22], Leibon[23], Chow and Luo[7], Bobenko and Springborn[24], Guo and Luo[25], and Springborn[26]. Variational principles for polyhedral surfaces including the topic of circle packing were studied systematically by Luo[27]. Many energy functions are derived from the cosine law and its derivative. Tangent circle packing is generalized to tangent circle packing with a family of discrete curvature. For the exposition of this work, see also [28].

3 Smooth Surface Ricci Flow

This section briefly reviews the fundamental concepts and theorems related to surface Ricci flow. Detailed discussion on Ricci flow on general Riemannian manifolds can be found in [29]. Advanced topics on differential geometry related to Yamabe equations can be found in [30].

3.1 Isothermal Coordinates and Gauss-Bonnet Theorem

Given a metric surface, one can choose *isothermal coordinates* to facilitate geometric computations, as show in Fig.3. Most differential operators, such as gradient and Laplace-Beltrami operators, have the simplest form under isothermal coordinates.

Definition 1 (Isothermal Coordinates). *On a surface S with a Riemannian metric $\boldsymbol{g}$, a local coordinates system (u, v) is an isothermal coordinate system, if*

$$\boldsymbol{g}(u, v) = e^{2\lambda(u,v)}(du^2 + dv^2),$$

where $\lambda : S \to \mathbb{R}$ is a function defined on the surface and called conformal factor.

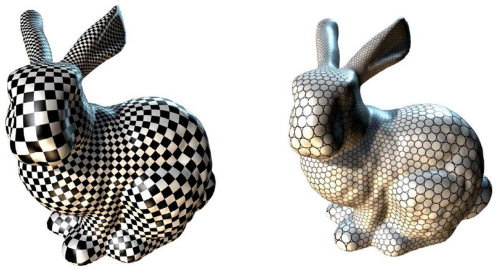

Fig.3. Isothermal coordinate system on the Stanford bunny surface. The mapping from the surface to the parameter plane is conformal, which preserves angles and infinitesimal circles[31].

Isothermal coordinates on metric surfaces always exist, and can be proved using either surface Ricci flow or quasi-conformal mapping.

Under the isothermal coordinates, the Gaussian curvature can be formulated as

$$K(u, v) = -e^{-2\lambda(u,v)}\left(\frac{\partial^2}{\partial u^2} + \frac{\partial^2}{\partial v^2}\right)\lambda = -\Delta_{\boldsymbol{g}}\lambda,$$

where the Laplace-Beltrami operator is

$$\Delta_{\boldsymbol{g}} = e^{-2\lambda(u,v)}\left(\frac{\partial^2}{\partial u^2} + \frac{\partial^2}{\partial v^2}\right).$$

The Gauss-Bonnet theorem claims that although the Gauss curvature is determined by the Riemannian metric, the total curvature is solely determined by the surface topology.

Theorem 1 (Gauss-Bonnet). *Suppose S is a compact 2D Riemannian manifold with piecewise-smooth boundary ∂S. Let K be the Gaussian curvature, k_g the geodesic curvature of ∂S, and $\theta_k, k = 1, 2 \cdots, n$, the exterior angles of ∂S. Then*

$$\int_S K \mathrm{d}A + \int_{\partial S} k_g \mathrm{d}s + \sum_{k=1}^{n} \theta_k = 2\pi\chi(S),$$

where $\chi(S)$ is the Euler characteristics of the surface.

3.2 Yamabe Problem

Suppose S is a surface with a Riemannian metric $\boldsymbol{g}$, which induces Gauss curvature K and geodesic curvature k_g on the boundary. Let

$$\bar{\boldsymbol{g}} = e^{2\lambda}\boldsymbol{g}$$

be another metric conformal to the original one, which induces Gauss curvature $\bar{K}$ and geodesic curvature $\bar{k}_g$. Then the relations between Gaussian curvature associated with a conformal change of metric are

$$\begin{aligned} \bar{K} &= e^{-2\lambda}(K - \Delta_{\boldsymbol{g}}\lambda), \\ \bar{k}_g &= e^{-\lambda}(k_g - \partial_{\boldsymbol{n},\boldsymbol{g}}\lambda). \end{aligned}$$

$\partial_{\boldsymbol{n},\boldsymbol{g}}$ can also written as $(\nabla_{\boldsymbol{g}}\lambda, \boldsymbol{n})$, $\nabla_{\boldsymbol{g}} = e^{-\lambda}(\frac{\partial}{\partial u}, \frac{\partial}{\partial v})$, $\boldsymbol{n} = (\sin\theta, -\cos\theta)$.

Problem 1 (Surface Yamabe Problem). *Given $(S, \boldsymbol{g})$ and the prescribed curvature, $\bar{K}$ and $\bar{k}_g$, compute the conformal factor λ.*

Surface Yamabe problem can be solved using surface Ricci flow.

3.3 Surface Ricci Flow

Given an n-dimensional Riemannian manifold M with metric tensor $\boldsymbol{g} = (g_{ij})$, the normalized Ricci flow is defined by the geometric evolution equation

$$\partial_t \boldsymbol{g}(t) = -2Ric(\boldsymbol{g}(t)) + \rho \boldsymbol{g}(t),$$

where Ric is the Ricci curvature tensor and ρ is the mean value of the scalar curvature

$$\rho = \frac{2}{n}\frac{\int_M R_{\boldsymbol{g}} \mathrm{d}\mu_{\boldsymbol{g}}}{\int_M \mathrm{d}\mu_{\boldsymbol{g}}},$$

where $R_{\boldsymbol{g}}$ and $\mu_{\boldsymbol{g}}$ are the scalar curvature and the volume element with respect to the evolving metric $\boldsymbol{g}(t)$, respectively. Recall that a one-parameter family of metrics $\{\boldsymbol{g}(t)\}$, where $t \in [0, T)$ for some $0 < T \leqslant \infty$, is called a solution to the normalized Ricci flow if it satisfies the above equation at all $p \in M$ and $t \in [0, T)$.

In two dimensions, the Ricci curvature for a metric $\boldsymbol{g}$ is equal to $\frac{1}{2}R\boldsymbol{g}$, where R is the scalar curvature (or twice the Gauss curvature). Therefore, the normalized Ricci flow equation for surfaces takes the form

$$\partial_t \boldsymbol{g}(t) = (\rho - R(t))\boldsymbol{g}(t), \tag{1}$$

where ρ is the mean value of the scalar curvature,

$$\rho = \frac{4\pi\chi(M)}{A(0)},$$

where $\chi(M)$ is the Euler characteristic number of M, and $A(0)$ is the total area of the surface M at time $t = 0$.

The normalized Ricci flow preserves the total area, $A(t) = A(0), \forall t > 0$. During the Ricci flow (1), the metric deforms conformally, $\boldsymbol{g}(t) = e^{2\lambda(t)}\boldsymbol{g}(0)$, the conformal factor evolution equation is

$$\partial_t \lambda = \frac{1}{2}(\rho - R),\ \lambda(0) = 0,$$

and the curvature evolution equation is

$$\partial_t R = \Delta_{\boldsymbol{g}(t)} R + R(R - \rho).$$

Hamilton[32] and Chow[33] proved the convergence of surface Ricci flow.

Theorem 2 (Hamilton[32]). *Let (M^2, g_0) be compact. If $\rho \leqslant 0$, or if $R(0) \geqslant 0$ on all of M^2, then the solution to (1) exists for all $t \geqslant 0$ and converges to a metric of constant curvature.*

Theorem 3 (Chow[33]). *If g_0 is any metric on $\mathbb{S}^2$, then its evolution under (1) develops positive scalar curvature in finite time, and hence by Theorem 2 converges to the round metric as t goes to ∞.*

Theorem 4. *Suppose $(S, \boldsymbol{g})$ is a compact, there is a function $\lambda : S \to \mathbb{R}$, such that $e^{2\lambda}\boldsymbol{g}$ induces constant Gaussian curvature. If the Euler characteristics of S $\chi(S)$ is positive, zero or negative, the constant is $+1, 0$ or -1 respectively.*

4 Unified Discrete Surface Ricci Flow

This section systematically introduces the unified framework for discrete surface Ricci flow. The whole theory is explained using the variational principle on discrete surfaces based on derivative cosine law[28]. The elementary concepts and some of schemes can be found in [27] and the chapter 4 in [1].

4.1 Discrete Surfaces

In practice, smooth surfaces are usually approximated by *discrete surfaces*. Discrete surfaces are represented as 2D simplicial complexes which are manifolds, as shown in Fig.4.

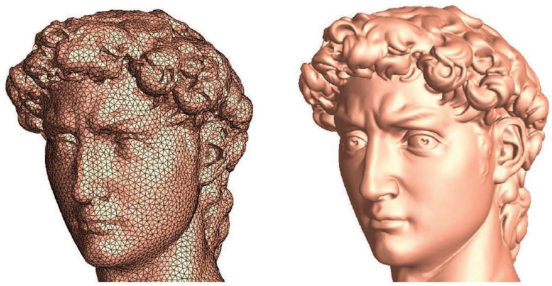

Fig.4. Smooth surfaces are approximated by discrete surfaces[31].

Definition 2 (Triangular Mesh). *Suppose Σ is a 2D simplicial complex, furthermore it is also a manifold, namely, for each point p of Σ, there exists a neighborhood of p, $U(p)$, which is homeomorphic to the whole plane or the upper half plane. Then Σ is called a triangular mesh. If $U(p)$ is homeomorphic to the whole plane, then p is called an interior point; if $U(p)$ is homeomorphic to the upper half plane, then p is called a boundary point.*

The fundamental concepts from smooth differential geometry, such as Riemannian metric, curvature and conformal structure, are generalized to the simplicial complex, respectively.

In the following discussion, we use $\Sigma = (V, E, F)$ to denote the mesh with vertex set V, edge set E, and face set F. A discrete surface is with Euclidean (hyperbolic or spherical) background geometry if it is constructed by isometrically gluing triangles in $\mathbb{E}^2$ ($\mathbb{H}^2$ or $\mathbb{S}^2$).

Definition 3 (Discrete Riemannian Metric). *A discrete metric on a triangular mesh is a function defined on the edges, $l : E \to \mathbb{R}^+$, which satisfies the triangle inequality: on each face (v_i, v_j, v_k), l_i, l_j, l_k are the lengths of edges against v_i, v_j, v_k respectively,*

$$l_i + l_j > l_k,\ l_j + l_k > l_i,\ l_k + l_i > l_j.$$

A triangular mesh with a discrete Riemannian metric is called a discrete metric surface.

Definition 4 (Background Geometry). *Suppose Σ is a discrete metric surface, if each face of Σ is a spherical, (Euclidean or hyperbolic) triangle, then we say Σ is with spherical (Euclidean or hyperbolic) background geometry. We use $\mathbb{S}^2$, $\mathbb{E}^2$ and $\mathbb{H}^2$ to represent spherical, Euclidean and hyperbolic background metric respectively.*

Triangles with different background geometries satisfy different cosine laws (Fig.5):

$$\mathbb{E}^2 : 1 = \frac{\cos\theta_i + \cos\theta_j \cos\theta_k}{\sin\theta_j \sin\theta_k},$$

$$\mathbb{S}^2 : \cos l_i = \frac{\cos\theta_i + \cos\theta_j \cos\theta_k}{\sin\theta_j \sin\theta_k},$$

$$\mathbb{H}^2 : \cosh l_i = \frac{\cosh\theta_i + \cosh\theta_j \cosh\theta_k}{\sinh\theta_j \sinh\theta_k}.$$

The discrete Gaussian curvature is defined as angle deficit, as shown in Fig.6.

Definition 5 (Discrete Gauss Curvature). *The discrete Gauss curvature function on a mesh is defined on vertices, $K : V \to \mathbb{R}$,*

$$K(v) = \begin{cases} 2\pi - \sum_{jk} \theta_i^{jk}, & \text{if } v \notin \partial M, \\ \pi - \sum_{jk} \theta_i^{jk}, & \text{if } v \in \partial M, \end{cases}$$

where θ_i^{jk} is the corner angle at v_i in the face (v_i, v_j, v_k), and ∂M represents the boundary of the mesh.

The Gauss-Bonnet theorem still holds in the discrete case.

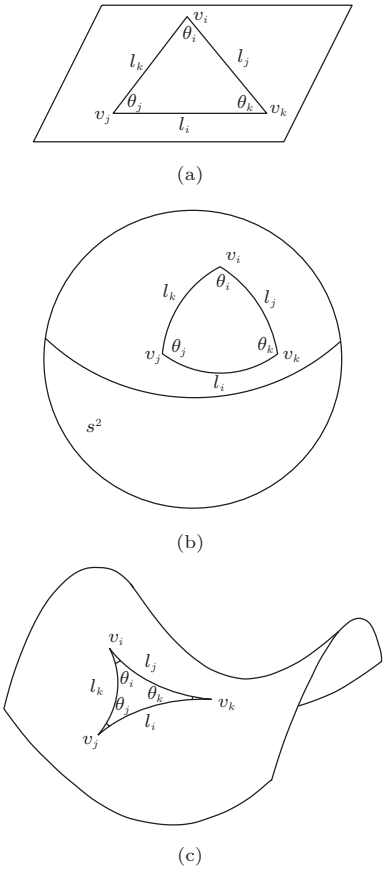

Fig.5. Different background geometries[20]. (a) Euclidean $\mathbb{E}^2$. (b) Spherical $\mathbb{S}^2$. (c) Hyperbolic $\mathbb{H}^2$.

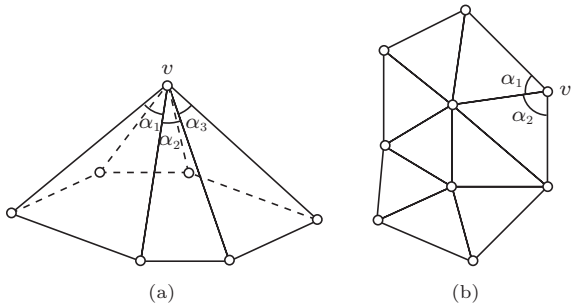

Fig.6. Discrete curvatures of an interior vertex and a boundary vertex[1].

Theorem 5 (Discrete Gauss-Bonnet Theorem). *Suppose Σ is a triangular mesh with Euclidean background metric. The total curvature is a topological invariant,*

$$\sum_{v \notin \partial\Sigma} K(v) + \sum_{v \in \partial\Sigma} K(v) + \epsilon A(\Sigma) = 2\pi\chi(\Sigma), \qquad (2)$$

where χ is the characteristic Euler number, K is the Gauss curvature, $A(\Sigma)$ is the total area, and $\epsilon = \{+1, 0, -1\}$ if Σ is with spherical, Euclidean or hyperbolic background geometry.

4.2 Unified Circle Packing Metrics

Definition 6 (Circle Packing Metric)**.** *Suppose $\Sigma = (V, E, F)$ is a triangle mesh with spherical, Euclidean or hyperbolic background geometry. Each vertex v_i is associated with a circle with radius γ_i. The circle radius function is denoted as $\gamma : V \to \mathbb{R}_{>0}$; a function defined on the vertices $\epsilon : V \to \{+1, 0, -1\}$ is called the scheme coefficient; a function defined on edges $\eta : E \to \mathbb{R}$ is called the discrete conformal structure coefficient. A circle packing metric is a 4-tuple $(\Sigma, \gamma, \eta, \epsilon)$, and the edge length is determined by the 4-tuple and the background geometry.*

In the smooth case, changing a Riemannian metric by a scalar function, $\boldsymbol{g} \to e^{2u}\boldsymbol{g}$, is called a conformal metric deformation. The discrete analogy to this is as follows.

Definition 7 (Discrete Conformal Equivalence)**.** *Two circle packing metrics $(\Sigma_k, \gamma_k, \eta_k, \epsilon_k)$, $k = 1, 2$, are conformally equivalent if $\Sigma_1 = \Sigma_2$, $\eta_1 = \eta_2$, $\epsilon_1 = \epsilon_2$. (γ_1 may not equal γ_2.)*

The discrete analogy to the concept of conformal factor in the smooth case is:

Definition 8 (Discrete Conformal Factor)**.** *Discrete conformal factor for a circle packing metric $(\Sigma, \gamma, \eta, \epsilon)$ is a function defined on each vertex $\boldsymbol{u} : V \to \mathbb{R}$,*

$$u_i = \begin{cases} \log \gamma_i, & \mathbb{E}^2, \\ \log \tanh \frac{\gamma_i}{2}, & \mathbb{H}^2, \\ \log \tan \frac{\gamma_i}{2}, & \mathbb{S}^2. \end{cases}$$

Definition 9 (Circle Packing Schemes)**.** *Suppose $\Sigma = (V, E, F)$ is triangle mesh with spherical, Euclidean or hyperbolic background geometry. Given a circle packing metric $(\Sigma, \gamma, \eta, \epsilon)$, for an edge $(v_i, v_j) \in E$, its length l_{ij} is given by*

$$\begin{cases} l_{ij}^2 = 2\eta_{ij} e^{u_i+u_j} + \varepsilon_i e^{2u_i} + \varepsilon_j e^{2u_j}, & \mathbb{E}^2, \\ \cosh l_{ij} = \frac{4\eta_{ij} e^{u_i+u_j} + (1+\varepsilon_i e^{2u_i})(1+\varepsilon_j e^{2u_j})}{(1-\varepsilon_i e^{2u_i})(1-\varepsilon_j e^{2u_j})}, & \mathbb{H}^2, \\ \cos l_{ij} = \frac{-4\eta_{ij} e^{u_i+u_j} + (1-\varepsilon_i e^{2u_i})(1-\varepsilon_j e^{2u_j})}{(1+\varepsilon_i e^{2u_i})(1+\varepsilon_j e^{2u_j})}, & \mathbb{S}^2. \end{cases} \quad (3)$$

The schemes are named in Table 1.

Table 1. Scheme Name

Scheme	ε_i	ε_j	η_{ij}
Tangential circle packing	$+1$	$+1$	$+1$
Thurston's circle packing	$+1$	$+1$	$[0, 1]$
Inversive distance circle packing	$+1$	$+1$	> 0
Yamabe flow	0	0	> 0
Virtual radius circle packing	-1	-1	> 0
Mixed type	$\{-1, 0, +1\}$	$\{-1, 0, +1\}$	> 0

Fig.7 illustrate all the schemes with discrete surfaces with Euclidean background geometry.

From the definition, the tangential circle packing is a special case of Thurston's circle packing; Thurston's circle packing is a special case of inversive distance circle packing. In the following discussion, we unify all three types as inversive distance circle packing.

4.3 Discrete Surface Ricci Flow

Definition 10 (Discrete Surface Ricci Flow)**.** *For a discrete surface with $\mathbb{S}^2$, $\mathbb{E}^2$ or $\mathbb{H}^2$ background geometry, and a circle packing metric $(\Sigma, \gamma, \eta, \epsilon)$, the discrete surface Ricci flow is*

$$\frac{du_i(t)}{dt} = \bar{K}_i - K_i(t),$$

where $\bar{K}_i$ is the target curvature at the vertex v_i.

The target curvature must satisfy certain constraints to ensure the existence of the solution to the flow, such as Gauss-Bonnet equation (2), and some additional ones described in [2], [7], and [8], for instance.

The discrete surface Ricci flow has exactly the same formula as the smooth counterpart (1). Furthermore, similar to the smooth case, discrete surface Ricci flow is also variational: the discrete Ricci flow is the negative gradient flow of the discrete Ricci energy.

Definition 11 (Discrete Ricci Energy)**.** *Given a discrete surface with $\mathbb{S}^2$, $\mathbb{E}^2$ or $\mathbb{H}^2$ background geometry, and a circle packing metric $(\Sigma, \gamma, \eta, \epsilon)$, for a triangle (v_i, v_j, v_k) with inner angles $(\theta_i, \theta_j, \theta_k)$, the discrete Ricci energy on the face is given by*

$$E_f(u_i, u_j, u_k) = \int^{(u_i,u_j,u_k)} \theta_i \mathrm{d}u_i + \theta_j \mathrm{d}u_j + \theta_k \mathrm{d}u_k. \quad (4)$$

The discrete Ricci energy for the whole mesh is defined as

$$E_\Sigma(u_1, u_2, \cdots, u_n) = \int^{(u_1,u_2,\cdots,u_n)} \sum_{i=1}^{n} (\bar{K}_i - K_i)\mathrm{d}u_i.$$

From Definition 11, we get the relation between the surface Ricci energy and the face Ricci energy:

$$E_\Sigma = \sum_{i=1}^{n} (\bar{K}_i - 2\pi)u_i + \sum_{f \in F} E_f.$$

The description of the energy in terms of an integral requires the fact that the intergrand is a closed form so that it is defined independent of the integration path. This follows from the following symmetry lemma, which has fundamental importance. The proof is given by the geometric interpretation of the Ricci energy.

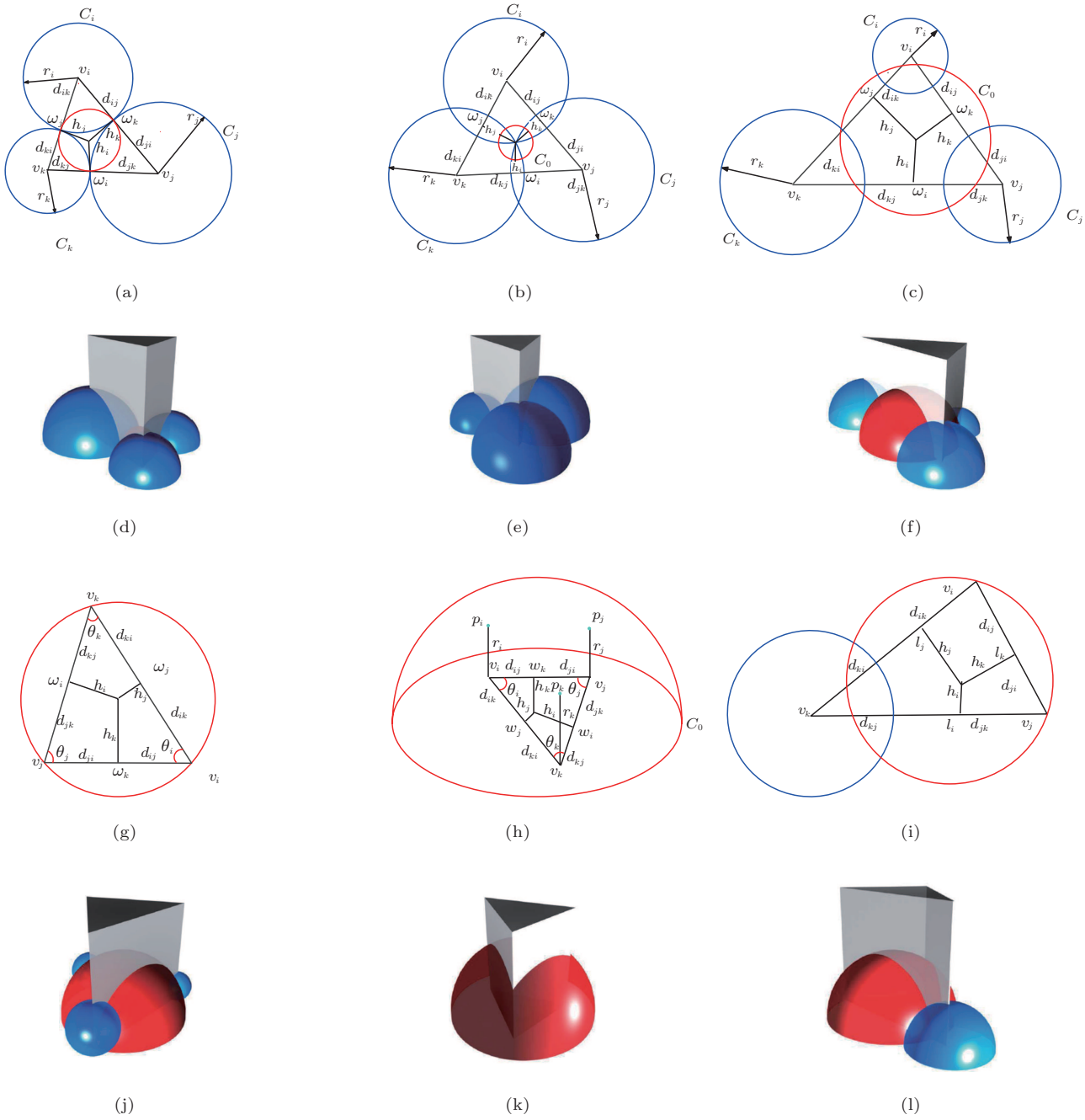

Fig.7. Circle packing (CP) schemes and the geometric interpretation to their Ricci energies[20]. (a) Tangential CP. (b) Thurston's CP. (c) Inversive distance CP. (d) Tangential CP, $\eta = 1$, $\epsilon = 1$. (e) Thurston's CP, $0 \leqslant \eta \leqslant 1$, $\epsilon = 1$. (f) Inversive distance CP, $\eta \geqslant 1$, $\epsilon = 1$. (g) Yamabe flow. (h) Virtual radius CP (virt.rad.cp). (i) Mixed type. (j) Yamabe flow, $\eta > 0$, $\epsilon = 0$. (k) Virt.rad.cp, $\eta > 0$, $\epsilon = -1$. (l) Mixed type, $\eta > 0$, $\epsilon \in \{+1, 0, -1\}$.

Lemma 1 (Symmetry). *Given a discrete surface with $\mathbb{S}^2$, $\mathbb{E}^2$ or $\mathbb{H}^2$ background geometry, and a circle packing metric $(\Sigma, \gamma, \eta, \epsilon)$, it has for any pair of vertices v_i and v_j:*

$$\frac{\partial K_i}{\partial u_j} = \frac{\partial K_j}{\partial u_i}.$$

4.4 Geometric Interpretations to Ricci Energies

This subsection focuses on the geometric interpretation to Ricci energies of all the schemes in all background geometries, as shown in Fig.8.

We use the upper half space model for $\mathbb{H}^3$, with

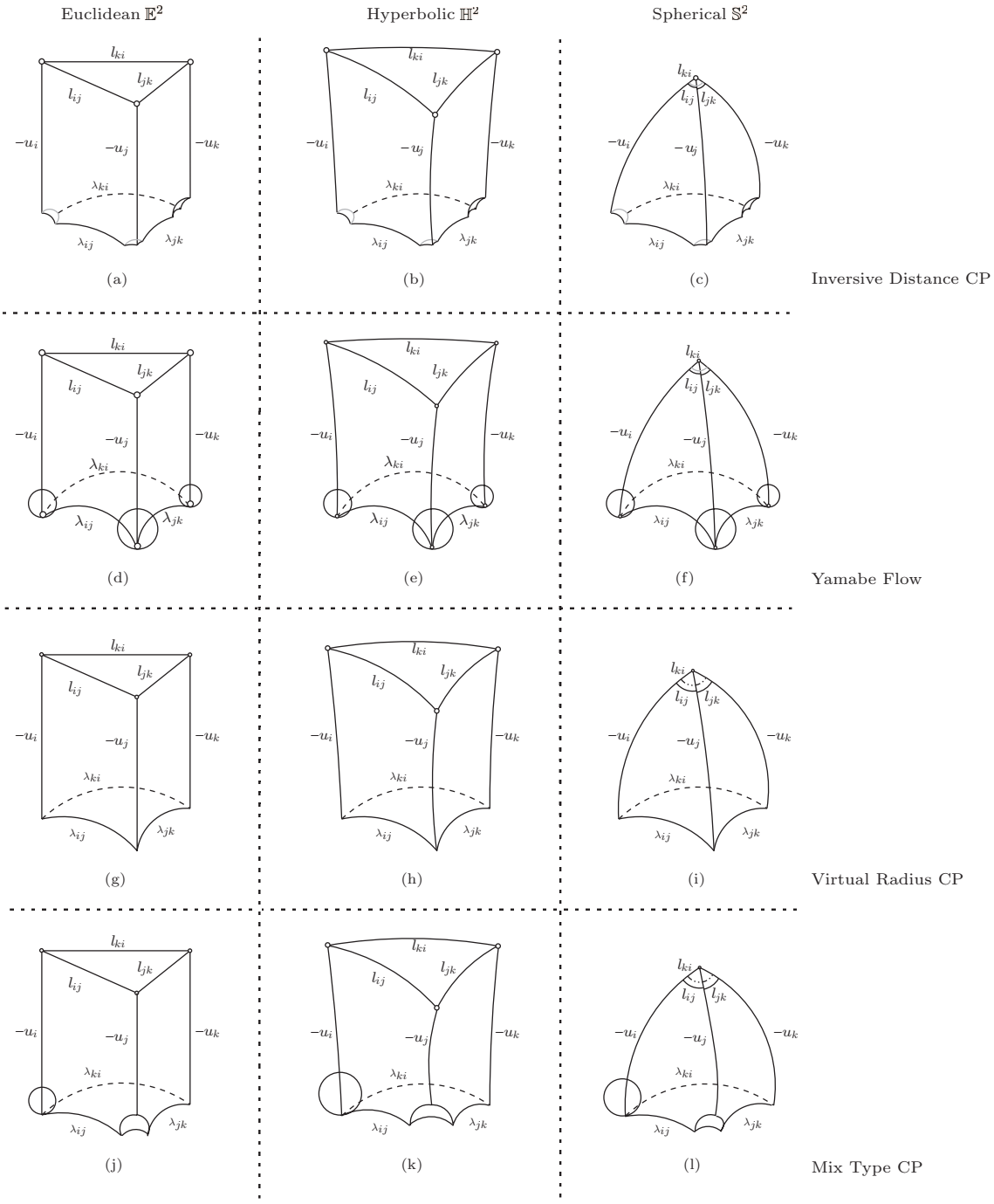

Fig.8. Geometric interpretation to discrete Ricci energy — volumes of generalized hyperbolic tetrahedra[20]. Inversive distance circle packing in (a) Euclidean $\mathbb{E}^2$, (b) hyperbolic $\mathbb{H}^2$, (c) spherical $\mathbb{S}^2$. Yamabe flow in (d) $\mathbb{E}^2$, (e) $\mathbb{H}^2$, (f) $\mathbb{S}^2$. Virtual radius circle packing in (g) $\mathbb{E}^2$, (h) $\mathbb{H}^2$, (i) $\mathbb{S}^2$. Mixed type schemes in (j) $\mathbb{E}^2$, (k) $\mathbb{H}^2$, (l) $\mathbb{S}^2$.

Riemannian metric

$$\mathrm{d}s^2 = \frac{\mathrm{d}x^2 + \mathrm{d}y^2 + \mathrm{d}z^2}{z^2},$$

and the xy-plane is the ideal boundary. Consider a triangle (v_i, v_j, v_k), its Ricci energy is closely related to the volume of a generalized hyperbolic tetrahedron whose vertices can be in $\mathbb{H}^3$, truncated by a horosphere or truncated by a hyperbolic plane.

In Fig.9, the generalized hyperbolic tetrahedron has four vertices w_0, w_i, w_j, w_k. The tetrahedron vertex w_0 is called the top vertex. The four faces of the tetrahedron are hyperbolic planes, and the six edges are

geodesics. The six edge lengths of the generalized tetrahedron are $-u_i, -u_j, -u_k$ and $\lambda_{ij}, \lambda_{jk}, \lambda_{ki}$ respectively. The generalized tetrahedron is uniquely determined by these six edge lengths.

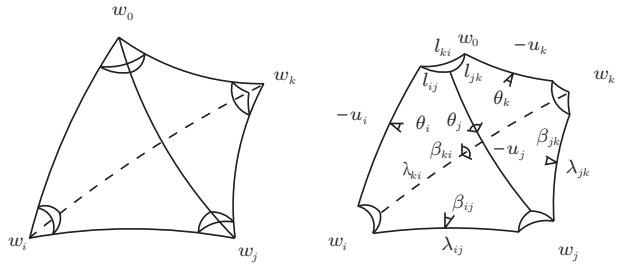

Fig.9. Generalized hyperbolic tetrahedron[20].

The followings are the common principles for constructing the generalized tetrahedron for all the schemes.

1) For all $\mathbb{E}^2$ schemes, the top vertex w_0 is ideal (at infinity) and truncated by a horosphere; for all $\mathbb{H}^2$ schemes, the top vertex is hyperideal (exceeding the boundary of $\mathbb{H}^3$) and truncated by a hyperbolic plane; for all $\mathbb{S}^2$ schemes, the top vertex is in $\mathbb{H}^3$.

2) For w_i, if the corresponding vertex v_i is of inversive distance circle packing $\varepsilon_i = +1$, then it is hyperideal and truncated by a hyperbolic plane; if v_i is of Yamabe flow $\varepsilon_i = 0$, then it is ideal and truncated by a horosphere; if v_i is virtual radius circle packing $\varepsilon_1 = -1$, then it is in $\mathbb{H}^3$. Same results hold for w_j and w_k.

3) The edges on the truncated tetrahedron, connecting to the top vertex on the original tetrahedron, have lengths $-u_i$, $-u_j$ and $-u_k$ respectively.

4) For the edge lengths λ_{ij}, there is a unified formula for three geometries: Euclidean, hyperbolic, spherical,

$$\eta_{ij} = \frac{1}{2}(e^{\lambda_{ij}} + \varepsilon_i\varepsilon_j e^{-\lambda_{ij}}).$$

The triangle associated with the top vertex w_0 is the triangle (v_i, v_j, v_k). It is obtained by truncating by a horosphere, truncating by a hyperbolic plane or intersecting with a sphere. Given $-u_i, -u_j, -u_k, \eta_{ij}, \eta_{jk}, \eta_{ki}$, using cosine law, we can calculate the edge lengths of the triangle (v_i, v_j, v_k). They are exactly given by (3). That means the triangle (v_i, v_j, v_k) has lengths l_{ij}, l_{jk}, l_{ki} and angles $\theta_i, \theta_j, \theta_k$.

Here we can give the proof for the symmetry lemma based on the geometric interpretation to the Ricci energy, which is more geometric, intuitive and much easier to verify.

Proof. As shown in Fig.8, for a generalized hyperbolic tetrahedron, the four vertices can have any types. The three vertical edges have lengths $-u_i, -u_j, -u_k$ with dihedral angles $\theta_i, \theta_j, \theta_k$. The bottom edges have lengths $\lambda_{ij}, \lambda_{jk}, \lambda_{ki}$ with dihedral angles $\beta_{ij}, \beta_{jk}, \beta_{ki}$.

Let V be the volume of the generalized hyperbolic tetrahedron. By the Schläfli formula

$$\begin{aligned} \mathrm{d}V &= -\frac{1}{2}(-u_i\mathrm{d}\theta_i - u_j\mathrm{d}\theta_j - u_k\mathrm{d}\theta_k + \\ &\quad \lambda_{ij}\mathrm{d}\beta_{ij} + \lambda_{jk}\mathrm{d}\beta_{jk} + \lambda_{ki}\mathrm{d}\beta_{ki}). \end{aligned} \tag{5}$$

During the Ricci flow, the conformal structure coefficients, $\eta_{ij}, \eta_{jk}, \eta_{ki}$, are invariant, thereby $\lambda_{ij}, \lambda_{jk}, \lambda_{ki}$ are fixed. Because the generalized tetrahedron is determined by the edge lengths $-u_i, -u_j, -u_k, \lambda_{ij}, \lambda_{jk}, \lambda_{ki}$, during the flow, all dihedral angles $\theta_i, \theta_j, \theta_k, \beta_{ij}, \beta_{jk}, \beta_{ki}$ are functions of u_i, u_j, u_k, and the volume V is also the function of u_i, u_j, u_k.

Consider the function,

$$\begin{aligned} W(u_i, u_j, u_k) &= u_i\theta_i + u_j\theta_j + u_k\theta_k - \lambda_{ij}\beta_{ij} - \\ &\quad \lambda_{jk}\beta_{jk} - \lambda_{ki}\beta_{ki} - 2V, \end{aligned} \tag{6}$$

hence,

$$\begin{aligned} \mathrm{d}W &= \theta_i\mathrm{d}u_i + \theta_j\mathrm{d}u_j + \theta_k\mathrm{d}u_k + u_i\mathrm{d}\theta_i + u_j\mathrm{d}\theta_j + \\ &\quad u_k\mathrm{d}\theta_k - \lambda_{ij}\mathrm{d}\beta_{ij} - \lambda_{jk}\mathrm{d}\beta_{jk} - \lambda_{ki}\mathrm{d}\theta_{ki} - 2\mathrm{d}V, \end{aligned}$$

substituting the Schläfli formula (5), we have

$$\mathrm{d}W = \theta_i\mathrm{d}u_i + \theta_j\mathrm{d}u_j + \theta_k\mathrm{d}u_k;$$

therefore

$$W = \int \theta_i\mathrm{d}u_i + \theta_j\mathrm{d}u_j + \theta_k\mathrm{d}u_k + c.$$

W, in fact, is the discrete Ricci energy on face in (4). This shows the differential 1-form

$$\theta_i\mathrm{d}u_i + \theta_j\mathrm{d}u_j + \theta_k\mathrm{d}u_k \tag{7}$$

is exact, therefore closed. Namely, the Hessian matrix

$$\frac{\partial(\theta_i, \theta_j, \theta_k)}{\partial(u_i, u_j, u_k)}$$

is symmetric. □

The formula (6) represents the Ricci energy on a face as the volume of the generalized hyperbolic tetrahedron with other terms of conformal factors and conformal structure coefficients. This formula was introduced first by Bobenko, Pinkall and Springborn in [34] for Euclidean and hyperbolic Yamabe flow. In the current work, we generalize it to all 18 schemes. The differential in (7) is independent of the choice of horospheres, since the Schläfli formula is independent of the choice of horospher for an ideal vertex.

4.5 Geometric Interpretation to Hessian

This subsection focuses on the geometric interpretation to Hessian matrix of the discrete Ricci energy on each face for the cases of $\mathbb{E}^2, \mathbb{H}^2$ and $\mathbb{S}^2$.

Euclidean Case. The interpretation in Euclidean case is due to Glickenstein[18] (He[35] in the case of circle packings) and illustrated in [1].

We only focus on one triangle (v_i, v_j, v_k), with corner angles $\theta_i, \theta_j, \theta_k$, conformal factors u_i, u_j, u_k and edge lengths l_{ij} for edge (v_i, v_j), l_{jk} for (v_j, v_k) and l_{ki} for (v_k, v_i).

As shown in Fig.7, the power of q with respect to v_i is

$$pow(v_i, q) = |v_i - q|^2 - \epsilon\gamma_i^2.$$

The power center o of the triangle satisifies

$$pow(v_i, o) = pow(v_j, o) = pow(v_k, o).$$

The power circle C is centered at o with radius γ, where $\gamma = pow(v_i, o)$.

Therefore, for tangential, Thurton's and inversive distance circle packing cases, the power circle is orthogonal to three circles at the vertices C_i, C_j and C_k; for Yamabe flow case, the power circle is the circumcircle of the triangle; for virtual radius circle packing, the power circle is the equator of the sphere, which goes through three points $\{v_i + \gamma_i \boldsymbol{n}, v_j + \gamma_j \boldsymbol{n}, v_k + \gamma_k \boldsymbol{n}\}$, where $\boldsymbol{n}$ is the normal to the plane.

Through the power center, we draw lines perpendicular to three edges, and the perpendicular feet are w_i, w_j and w_k respectively. The distances from the power center to the perpendicular feet are h_i, h_j and h_k respectively. Then it can be shown easily that

$$\begin{aligned}
\frac{\partial \theta_i}{\partial u_j} &= \frac{\partial \theta_j}{\partial u_i} = \frac{h_k}{l_k}, \\
\frac{\partial \theta_j}{\partial u_k} &= \frac{\partial \theta_k}{\partial u_j} = \frac{h_i}{l_i}, \\
\frac{\partial \theta_k}{\partial u_i} &= \frac{\partial \theta_i}{\partial u_k} = \frac{h_j}{l_j},
\end{aligned}$$

furthermore,

$$\begin{aligned}
\frac{\partial \theta_i}{\partial u_i} &= -\frac{h_k}{l_k} - \frac{h_j}{l_j}, \\
\frac{\partial \theta_j}{\partial u_j} &= -\frac{h_k}{l_k} - \frac{h_i}{l_i}, \\
\frac{\partial \theta_k}{\partial u_k} &= -\frac{h_i}{l_i} - \frac{h_j}{l_j}.
\end{aligned}$$

Hyperbolic Case. Similar to Euclidean case, the power circle can be defined directly. For the mixed type of discrete conformal geometry, the edge length l_k is given by

$$\begin{aligned}
&\cosh l_k \\
= \; & 4\eta_{ij} \frac{\sinh r_i}{(1-\epsilon_i)\cosh r_i + 1 + \epsilon_i} \times \\
& \frac{\sinh r_j}{(1-\epsilon_j)\cosh r_j + 1 + \epsilon_j} + \cosh^{\epsilon_i} r_i \cosh^{\epsilon_j} r_j.
\end{aligned}$$

According to the cosine law, the edge lengths l_i, l_j, l_k determine the angles $\theta_i, \theta_j, \theta_k$. Let h_i be the distance from the center of the power circle to the edge (v_i, v_j) whose length is l_k.

Theorem 6. *Let*

$$e^{u_i} = \frac{e^{r_i} - 1}{e^{r_i} + 1} = \tanh \frac{r_i}{2}.$$

Then

$$\frac{\partial \theta_1}{\partial u_2} = \frac{\partial \theta_2}{\partial u_1}$$

which is equal to

$$\begin{aligned}
&\frac{\tanh h_3}{\sinh^2 l_3} \times \\
&\sqrt{2\cosh^{\epsilon_1} r_1 \cosh^{\epsilon_2} r_2 \cosh l_3 - \cosh^{2\epsilon_1} r_1 - \cosh^{2\epsilon_2} r_2}.
\end{aligned}$$

The detailed proof can be found in [20].

Spherical Case. According to a general principle of the relation of hyperbolic geometry and spherical geometry, to obtain a formula in spherical geometry, we only need to replace sinh and cosh in hyperbolic geometry by $\sqrt{-1}$ sin and cos.

Similar to the Euclidean case, the power circle can be defined directly. For the mixed type of discrete conformal geometry with spherical background geometry, the edge length of l_k is given by

$$\begin{aligned}
&\cosh l_{ij} \\
= \; & -4\eta_{ij} \frac{\sin r_i}{(1-\epsilon_i)\cos r_i + 1 + \epsilon_i} \times \\
& \frac{\sin r_j}{(1-\epsilon_j)\cos r_j + 1 + \epsilon_j} + \cos^{\epsilon_i} r_i \cos^{\epsilon_j} r_j.
\end{aligned}$$

Via the cosine law, the edge lengths l_i, l_j, l_k determine the angles $\theta_i, \theta_j, \theta_k$. Let h_i be the distance from the center of the power circle to the edge (v_i, v_j) whose length is l_k.

Theorem 7. *Let*

$$e^{u_i} = \tan \frac{r_i}{2}.$$

Then

$$\frac{\partial \theta_1}{\partial u_2} = \frac{\partial \theta_2}{\partial u_1}$$

which is equal to

$$\frac{\tan h_3}{\sin^2 l_3} \times \sqrt{-2\cos^{\epsilon_1} r_1 \cos^{\epsilon_2} r_2 \cos l_3 + \cos^{2\epsilon_1} r_1 + \cos^{2\epsilon_2} r_2}.$$

The detailed proof can be found in [20].

5 Applications for Surface Registration and Shape Analysis

The computational algorithms for discrete surface Ricci flow are straightforward, which optimize the discrete Ricci energy using Newton's method and preserve Delaunay triangulation. Due to the convexity of the energy, the computation is stable and efficient.

In order to compute the conformal metric with prescribed curvature, we can optimize the Yamabe energy using Newton's method. We give the discrete Yamabe flow as Algorithm 1.

Algorithm 1. Discrete Surface Yamabe Flow
Require:
1) a triangular mesh Σ, embedded in $\mathbb{E}^3$;
2) a target curvature $\bar{K}$, $\sum \bar{K}_i = 2\pi\chi(\Sigma)$ and $\bar{K}_i \in (-\infty, 2\pi)$
Ensure: a discrete metric conformal to the original one, which realizes the target curvature $\bar{K}$
Initialize the discrete conformal factor u as 0 and the conformal structure coefficient η, such that $\eta(e)$ equals the initial edge length of e
while $\max_i |\bar{K}_i - K_i| > threshold$ **do**
Compute the edge length from γ and η
Update the triangulation to be Delaunay using diagonal edge swap for each pair of adjacent faces
Compute the corner angle θ_i^{jk} from the edge length using cosine law
Compute the vertex curvature K
Compute the Hessian matrix $\boldsymbol{H}$
Solve linear system $\boldsymbol{H}\delta u = \bar{K} - K$
Update conformal factor $u \leftarrow u - \delta u$
end while
Output the result circle packing metric

Based on the uniformization theorem, surface can be mapped to Euclidean plane, sphere or hyperbolic disk. The computational method for genus 0 closed surface can be found in [31], the computational method for high genus closed surface can be found in [36], for genus 0 open surface, the computational details can be found in [37], and for high genus open surface, the computational details can be found in [1]. We also developed the unified Ricci flow algorithm[20].

Shape Registration and Tracking. They are the fundamental tasks in many engineering fields, including computer vision and medical imaging. Surface registration aims at finding a diffeomorphic mapping between two given surfaces with Riemannian metrics $(S_k, \boldsymbol{g}_k), k = 1, 2$, $\phi : (S_1, \boldsymbol{g}_1) \to (S_2, \boldsymbol{g}_2)$, such that the mapping preserves some geometric properties or optimizes some special form of energy $E(\phi)$. Surface tracking is to register two successive surface frames in a sequence of surfaces with dynamic deformations.

All the methods for surface registration and tracking share the same framework. By mapping 3D surfaces to canonical planar domains using Ricci flow, 3D geometric processing tasks can be converted to image processing problems. This greatly improves the efficiency and efficacy of computational algorithms. The framework of surface matching and registration can be summarized as the following diagram.

$$\begin{array}{ccc} S_1 & \xrightarrow{f} & S_2 \\ {\scriptstyle f_1}\downarrow & & \downarrow{\scriptstyle f_2} \\ D_1 & \xrightarrow{\phi} & D_2 \end{array}$$

Suppose $S_k, k = 1, 2$, are the input *source* and *target* surfaces, respectively. In order to compute the optimal diffeomorphism $f : S_1 \to S_2$, we conformally map them onto the plane by $f_k : S_k \to D_k$, where D_k are called *conformal parameter domains*, and then construct a planar diffeomorphism $\phi : D_1 \to D_2$. The registration between two surfaces is given by $f = f_2^{-1} \circ \phi \circ f_1$. Moreover, ϕ can be further optimized in the 2D mapping space. This provides a key to constructing the globally optimal diffeomorphism between surfaces.

Deformable Clothes Tracking. The clothes deformation is close to isometry. The deformable clothes tracking can be performed based on the registrations frame by frame. The clothes surfaces are captured by the 3D scanner introduced by [38]. Each frame is a topological quadrilateral (i.e., only one simple boundary with four corners), and can be mapped to a rectangle automatically by the Euclidean discrete surface Ricci flow. In order to verify if the deformation is close to be conformal/isometric, we compute the conformal module of each frame. The conformal modules are very consistent across the frames. This validates our hypothesis that the deformations are close to be conformal.

We also use vision techniques to find textural features on each frame, and use them as hard constraints for the registrations between two adjacent frames. The registration between two planar rectangles with feature point constraints is performed based on planar harmonic maps. Because the deformations are close to be conformal, the harmonic mappings are close to identity. In order to visualize the tracking results, we put

checker-board textures to the first frame, and propagate the texture parameters to the other frames through the correspondences from tracking. As shown in Fig.10, the checker-board textures are consistent across frames, without oscillating effects or checker collapse. This demonstrates that the registration between two frames is a diffeomorphism, and the tracking is stable and automatic.

Fig.10. Tracking for deformable clothes sequences. The consistent tracking results can be observed from the checker-board texture motion[1].

Human Face Registration with Expressions. In general, human facial expression changes are not conformal, and far away from isometry. This can be easily verified by computing the conformal modules of the same face with different expressions. The expression surfaces can be obtained from a real-time structured light 3D scanner[39]. For example, the face surfaces without interior regions of eyes and mouth are conformally mapped to the planar circle domains, and then by comparing the inner circle positions and sizes, one can tell the change of the conformal structures[40]. It is challenging to register the circle domains using harmonic maps, because the harmonic maps may not be diffeomorphic due to their concavities. Instead, we can apply hyperbolic Ricci flow and use hyperbolic harmonic map to ensure the diffeomorphic results. We can also use Euclidean Ricci flow to concentrate all the curvatures to some feature points, and set the Gauss curvature and the geodesic curvature to be zero everywhere. Then the surface can be decomposed to the union of planar convex polygons, and registered by piecewise harmonic maps. Details can be found in [40]. Fig.11 demonstrates the registration for a sequence of human facial surfaces with non-isometric deformations, complex topologies, and inconsistent boundaries. The one-to-one correspondence is visualized by the consistent checker-board texture mapping results.

Registration of Surfaces with Large Deformations. Quasi-conformal geometry provides a powerful approach to registration. The strategy for registration is first to estimate the Beltrami coefficient μ and then compute the quasi-conformal mapping under the auxiliary metric associated with μ. A coarse-to-fine method to compute μ is introduced in [41]. The Beltrami coefficient is estimated from the graph of feature points, and then refined by the diffusion on the whole surface. The Beltrami coefficient can also be obtained by minimizing the matching energy[42]. The methods can handle surfaces with complicated topologies and large anisometric deformations.

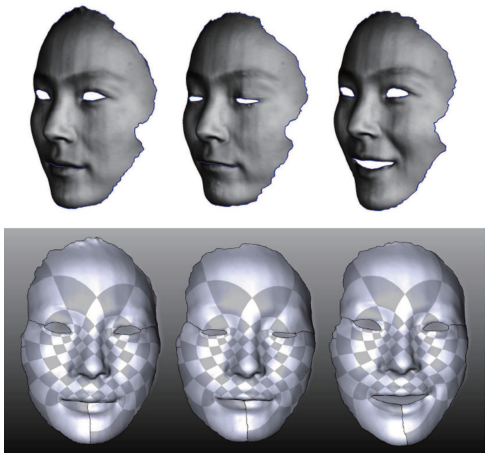

Fig.11. Registration for human facial surfaces with expression change by hyperbolic Ricci flow[1].

Fig.12 shows the registration between two facial surfaces of the same person with a large expression deformation. Both faces are mapped to the planar annuli conformally, and then the annuli are registered by a quasi-conformal mapping using the auxiliary metric method. The consistent circle-packing texture mapping demonstrates the one-to-one correspondence between two faces. From Fig.12, we can see that an ellipse field on the calm face is mapped to a circle field on the frightened face. Therefore, the mapping is quasi-conformal. The distortion can be visualized by the color encoded eccentricity and argument of the Beltrami coefficient.

Virtual Colonoscopy. Colorectal cancer is the third most incident cancer and the second leading cause of cancer-related mortality in the United States[43]. Optical colonoscopy (OC), whereby precancerous polyps can be located and removed, has been recommended for screening and has helped to greatly reduce the mortality rate of colorectal cancer[44]. Virtual colonoscopy (VC) techniques have been developed as viable non-invasive alternatives to OC for screening purposes[45-46]. The colon wall surface is reconstructed from CT images. By using Ricci flow, one can flatten the whole colon wall surface onto a planar rectangle[47].

Then polyps and other abnormalities can be found efficiently on the planar image by computer aided detection (CAD) techniques.

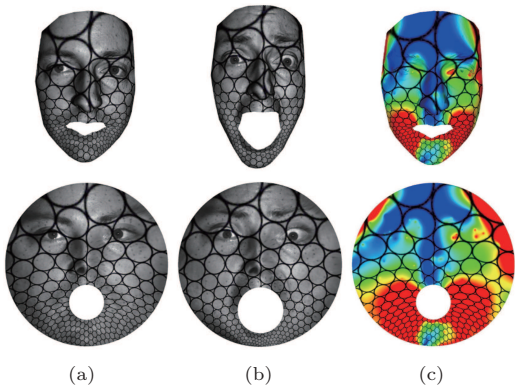

Fig.12. Quasi-conformal registration for a topological annulus case. The ellipse field on the source domain A is mapped to the circle field on the target domain B. The distortion is visualized by the eccentricity of ellipses $D(\mu)$ on both the 3D surface and its circle domain C, where the red color denotes the higher non-conformality, and the blue color denotes the higher conformality[1]. (a) Domain A. (b) Domain B. (c) Domain C.

For a VC procedure, CT scans of the abdomen are commonly acquired with the patient in both supine (facing up) and prone (facing down) positions. Being able to register these two scans is useful for a routine VC system to provide the user with the ability for confirming a finding or easy comparison when something might be unclear in one of the scans, and is also helpful for a CAD system to achieve greater accuracy while at the same time reducing false positive results. As shown in Fig.13, the colon surface is regarded as a topological cylinder, and therefore can be mapped to a rectangle using Euclidean Ricci flow. By quasi-conformal registration, we obtain the one-to-one correspondence between them, and then use that to analyze and visualize the elastic deformation of the colon. Details can be found in [48].

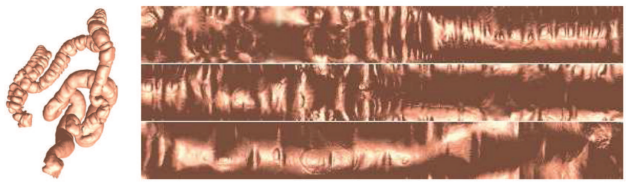

Fig.13. Colon wall surface flattening by using Euclidean Ricci flow. The rectangular flattened mapping is cut to 3 segments for display. Data courtesy of Arie E. Kaufman[1].

Brain Mapping. The human brain cortical surfaces can be reconstructed from CT images and discretized as triangular meshes. The brain cortical surface can be mapped to a canonical planar domain. All the geometric details are exposed onto the domain. The morphometry analysis can be constructed on the canonical domain. Besides, by using the landmarks on the brain, the brain surface is sliced open with holes, where each landmark generates a hole. Therefore, the brain cortical surface with holes can be mapped to either a circle domain where each hole is mapped to a circle, or a hyperbolic convex domain where each hole is mapped to a geodesic in hyperbolic space. The conformal modules can be extracted for brain surface shape analysis purposes. Fig.14 shows an example of hyperbolic mapping for a brain cortical surface with one boundary and three interior landmarks.

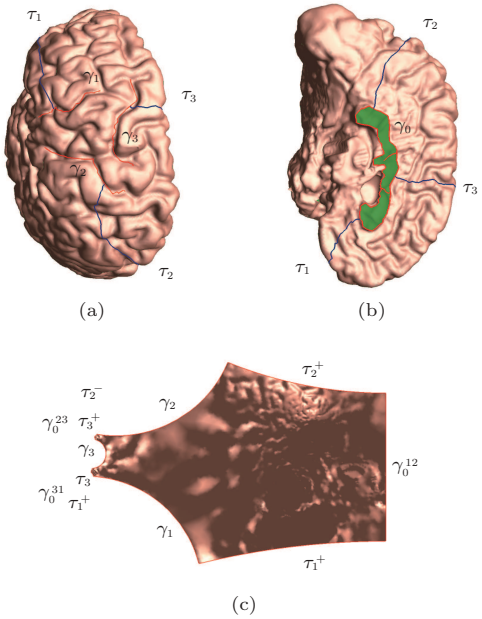

Fig.14. Brain mapping. A human brain surface with one boundary γ_0 (b) is sliced open by three interior landmarks $\gamma_k, k = 1, 2, 3$ (a), then it becomes a genus zero surface with four boundaries. By Hyperbolic Ricci flow, it is mapped to a hyperbolic convex polygon on Poincaré disk (c) where the domain is sliced open by curves $\tau_k, k = 1, 2, 3$ (b) between γ_0 and $\gamma_k, k = 1, 2, 3$, respectively[1].

It is crucial to register different brain cortical surfaces in brain imaging field. Since brain cortical surfaces are highly convoluted and different people have different anatomic structures, it is quite challenging to find a good registration (or mapping) between them. By finding an automorphism of the canonical shapes, the registration between surfaces can be easily established. The computation of the spherical, Euclidean, and hyperbolic brain mappings is based on the discrete

Ricci flow method. The details of brain surface mapping and its applications can be found in [49-50].

Human Facial Surface Dynamics. Suppose a sequence of facial surfaces with different expression changes are captured. By computing the time dependent conformal module $R(t)$, we can analyze the expression. Fig.15 shows such an example. A sequence of male facial surfaces from calm expression to frightened expression are acquired using a 3D camera system[39]. We remove the mouth region and compute the conformal module. It is easy to see that the human facial expression intensity is proportional to the norm of the conformal module. Details can be found in [51].

2D Shape Indexing and Retrieval. Shape analysis of objects from their observed silhouettes is important for many computer vision applications, such as classification, recognition and image retrieval. In real-world applications, objects from their observed silhouettes are usually multiply connected domains, i.e., domains with holes in the interior. Most of the existing methods work only on simple closed curves and generally cannot deal with multiply connected objects. Sharon and Mumford[52] proposed a conformal approach to model simple closed curves which captures subtle variability of shapes up to scaling and translation. They also introduced the Weil-Petersson metric on their proposed shape space. The method is generalized to represent multiple objects in a single image (i.e., with multiple contours) based on conformal welding signatures in [53]. The shape signature is complete and can represent 2D shapes with arbitrary topologies uniquely up to scalings and translations. As shown in Fig.16, the three different images with multiple boundaries have very different shape signatures. This demonstrates that the representation can be used to effectively classify 2D shapes.

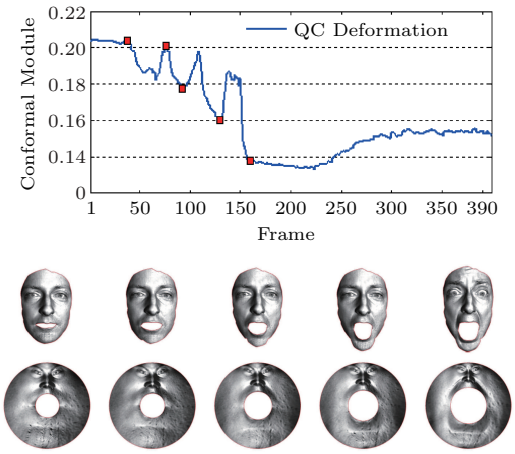

Fig.15. Conformal modules of a sequence of human facial surfaces with dynamic expressions. All the faces are mapped to a unit disk with one concentric circle with radius r. The conformal module is defined as $\frac{1}{2\pi}\log\frac{1}{r}$, which decreases monotonically as the inner circle radius increases[1].

6 Summary

Discrete surface Ricci flow is a powerful tool for designing Riemannian metrics by prescribed curvatures. It has elegant and profound theories and practical algorithms, and is valuable for both theoretic exploration and engineering applications.

We will continue to prove the existence and uniqueness of the solutions to discrete surface Ricci flow with general schemes and find broader applications in the future.

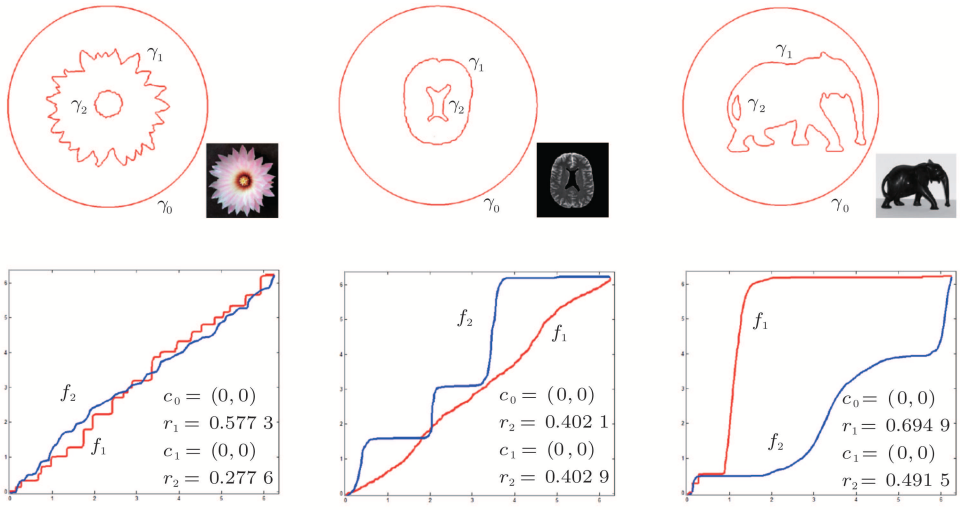

Fig.16. Conformal welding shape signatures of three different images with two levels of contours[1].

References

[1] Zeng W, Gu X. Ricci Flow for Shape Analysis and Surface Registration. Springer New York, 2013.

[2] Thurston W. The Geometry and Topology of 3-Manifolds. Princeton University Press, 1997.

[3] Andreev E M. Complex polyhedra in Lobačhevskiĭ spaces. *Mat. Sb.* (*N.S.*), 1970, 81(123): 445–478. (in Russian)

[4] Andreev E M. Convex polyhedra of finite volume in Lobačhevskiĭ space. *Mat. Sb.* (*N.S.*), 1970, 83(125): 256–260. (in Russian)

[5] Koebe P. Kontaktprobleme der konformen abbildung. *Ber. Sächs. Akad. Wiss. Leipzig, Math. Phys. Kl.*, 1936, 88: 141–164.

[6] Rodin B, Sullivan D. The convergence of circle packings to the Riemann mapping. *Journal of Differential Geometry*, 1987, 26(2): 349–360.

[7] Chow B, Luo F. Combinatorial Ricci flows on surfaces. *Journal of Differential Geometry*, 2003, 63(1): 97–129.

[8] Marden A, Rodin B. On Thurston's formulation and proof of Andreev's theorem. In *Lecture Notes in Math. 1435*, Ruscheweyh S, Satt E, Salinas L *et al.* (eds.), Springer Berlin, 1990, pp.103–116.

[9] Colin de Verdiére Y. Un principe variationnel pour les empilements de cercles. *Invent. Math.*, 1991, 104: 655–669.

[10] Stephenson K. Introduction to Circle Packing: The Theory of Discrete Analytic Functions. Cambridge University Press, 2005.

[11] He Z X, Schramm O. On the convergence of circle packings to the Riemann map. *Invent. Math.*, 1996, 125(2): 285–305.

[12] Bowers P L, Stephenson K. Uniformizing Dessins and Belyi Maps via Circle Packing. Amer. Math. Soc., 2004.

[13] Guo R. Local rigidity of inversive distance circle packing. *Trans. Amer. Math. Soc.*, 2011, 363: 4757–4776.

[14] Luo F. Combinatorial Yamabe flow on surfaces. *Contemp. Math.*, 2004, 6(5): 765–780.

[15] Springborn B, Schröder P, Pinkall U. Conformal equivalence of triangle meshes. *ACM Trans. Graph.*, 2008, 27(3): Article No. 77.

[16] Glickenstein D. A combinatorial Yamabe flow in three dimensions. *Topology*, 2005, 44(4): 791–808.

[17] Glickenstein D. A maximum principle for combinatorial Yamabe flow. *Topology*, 2005, 44(4): 809–825.

[18] Glickenstein D. Discrete conformal variations and scalar curvature on piecewise flat two and three dimensional manifolds. *Journal of Differential Geometry*, 2011, 87(2): 201–238.

[19] Guo R. Combinatorial Yamabe flow on hyperbolic surfaces with boundary. *Communications in Contemporary Mathematics*, 2011, 13(5): 827–842.

[20] Zhang M, Guo R, Zeng W, Luo F, Yau S T, Gu X. The unified surface Ricci flow. *Graphic Models*, 2014, 76(5): 321–339.

[21] Brägger W. Kreispackungen und triangulierugen. *Enseign. Math.*, 1992, 38: 201–217.

[22] Rivin I. Euclidean structures of simplicial surfaces and hyperbolic volume. *Ann. Math.*, 1994, 139: 553–580.

[23] Leibon G. Characterizing the Delaunay decompositions of compact hyperbolic surface. *Geom. & Topol.*, 2002, 6: 361–391.

[24] Bobenko A I, Springborn B A. Variational principles for circle patterns and Koebe's theorem. *Trans. Amer. Math. Soc.*, 2004, 356(2): 659–689.

[25] Guo R, Luo F. Rigidity of polyhedral surface, II. *Geom. & Topol.*, 2009, 13: 1265–1312.

[26] Springborn B. A variational principle for weighted Delaunay triangulation and hyperideal polyhedra. *Journal of Differential Geometry*, 2008, 78(2): 333–367.

[27] Luo F. Rigidity of polyhedral surfaces. *arXiv:math.GT/0612714*, 2006.

[28] Dai J, Gu X, Luo F. Variational Principles for Discrete Surfaces (Advanced Lectures in Mathematics). High Education Press and International Press, 2007.

[29] Chow B, Lu P, Ni L. Hamilton's Ricci Flow (Graduate Studies in Mathematics). American Mathematical Society, 2006.

[30] Schoen R, Yau S T. Lecture on Differential Geometry, Volume 1. International Press Incorporated, Boston, 1994.

[31] Gu X, Yau S T. Computational Conformal Geometry. International Press, 2008.

[32] Hamilton R. Ricci flow on surfaces. *Mathematics and General Relativity, Contemporary Mathematics AMS, Providence, RI*, 1988, 71: 237–262.

[33] Chow B. The Ricci flow on the 2-sphere. *Journal of Differential Geometry*, 1991, 33(2): 325–334.

[34] Bobenko A, Pinkall U, Springborn B. Discrete conformal maps and ideal hyperbolic polyhedra. *arXiv:1005.2698*, 2013.

[35] He Z. Rigidity of infinite disk patterns. *Ann. Math.*, 1999 149(1): 1–33.

[36] Jin M, Kim J, Luo F, Gu X. Discrete surface Ricci flow. *IEEE Transactions on Visualization and Computer Graphic*, 2008, 14(5): 1030–1043.

[37] Zeng W, Yin X, Zhang M, Luo F, Gu X. Generalized Koebe's method for conformal mapping multiply connected domains. In *Proc. SIAM/ACM Joint Conference on Geometric and Physical Modeling*, Oct. 2009, pp.89–100.

[38] Hernandez C, Vogiatzis G, Brostow G J, Stenger B, Cipolla R. Non-rigid photometric stereo with colored lights. In *Proc. the 11th IEEE International Conference on Computer Vision*, Oct. 2007.

[39] Wang Y, Gupta M, Zhang S, Wang S, Gu X, Samaras D, Huang P. High resolution tracking of non-rigid motion of densely sampled 3D data using harmonic maps. *International Journal of Computer Vision*, 2008, 76(3): 283–300.

[40] Zeng W, Samaras D, Gu X. Ricci flow for 3D shape analysis. *IEEE Transactions on Pattern Analysis and Machine Intelligence*, 2010, 32(4): 662–677.

[41] Zeng W, Gu X. Registration for 3D surfaces with large deformations using quasi-conformal curvature flow. In *Proc. IEEE Conference on Computer Vision and Pattern Recognition*, June 2011, pp.2457–2464.

[42] Lui L M, Wong T, Zeng W, Gu X, Thompson P, Chan T, Yau S T. Optimization of surface registrations using Beltrami holomorphic flow. *Journal of Scientific Computing*, 2012, 50(3): 557–585.

[43] Horner M, Ries L, Krapcho M, Neyman N, Aminou R, Howlader N, Altekruse S, Feuer E, Huang L, Mariotto A, Miller B, Lewis D, Eisner M, Stinchcomb D, Edwards B. SEER cancer statistics review, 1975-2006. http://seer.cancer.gov/csr/1975_2006/, Apr. 2015.

[44] Center M, Jemal A, Smith R A, Ward E. Worldwide variations in colorectal cancer. *CA: A Cancer Journal for Clinicians*, 2009, 59(6): 366–378.

[45] Hong L, Muraki S, Kaufman A, Bartz D, He T. Virtual voyage: Interactive navigation in the human colon. In *Proc. the 24th ACM SIGGRAPH*, Aug. 1997, pp.27–34.
[46] Johnson C, Dachman A. CT colography: The next colon screening examination. *Radiology*, 2000, 216(2): 331–341.
[47] Qiu F, Fan Z, Yin X, Kauffman A, Gu X. Colon flattening with discrete Ricci flow. In *Proc. International Conference on Medical Image Computing and Computer Assisted Intervention*, Sept. 2009.
[48] Zeng W, Marino J, Chaitanya Gurijala K, Gu X, Kaufman A. Supine and prone colon registration using quasiconformal mapping. *IEEE Transactions on Visualization and Computer Graphics*, 2010, 16(6): 1348–1357.
[49] Gu X, Wang Y, Chan T, Thompson P M, Yau S T. Genus zero surface conformal mapping and its application to brain surface mapping. *IEEE Transactions on Medical Imaging*, 2004, 23(8): 949–958.
[50] Wang Y, Shi J, Yin X, Gu X, Chan T, Yau S T, Toga A W, Thompson P M. Brain surface conformal parameterization with the Ricci flow. *IEEE Transactions on Medical Imaging*, 2012, 31(2): 251–264.
[51] Zeng W, Gu X. 3D dynamics analysis in Teichmüller space. In *Proc. ICCV Workshops*, Nov. 2011, pp. 1610–1617.
[52] Sharon E, Mumford D. 2D-shape analysis using conformal mapping. *International Journal of Computer Vision*, 2006, 70(1): 55–75.
[53] Lui L M, Zeng W, Chan T F, Yau S T, Gu X. Shape representation of planar objects with arbitrary topologies using conformal geometry. In *Proc. the 11th European Conference on Computer Vision*, Sept. 2010.

Min Zhang received her B.S. and Ph.D. degrees in mathematics from Zhejiang University, Hangzhou. She got her second Ph.D. degree in the Department of Computer Science of the State University of New York at Stony Brook, USA, in 2014. Her research interests include computer graphics, visualization, and geometric modeling.

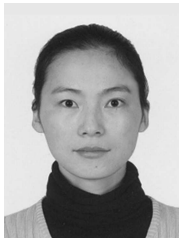

Wei Zeng is an assistant professor in School of Computing and Information Sciences at Florida International University. Dr. Zeng received her Ph.D. degree from Chinese Academy of Sciences in 2008 and had her postdoctoral training at Stony Brook University during 2010∼2012. Her research interests include computational conformal and quasiconformal geometry, discrete Ricci flow, Teichmüller theory, and their applications to surface matching, registration, tracking, recognition, and shape analysis. Her research areas span over medical imaging, computer vision, computer graphics and visualization, wireless sensor network, geometric modeling and computational topology. She has published numerous papers in peer-reviewed journals and conferences, won a Best Paper Award in CAD/CAM (IJCC 2009), and has two U.S. patents on virtual colonoscopy techniques.

Ren Guo received his Ph.D. degree in mathematics from Rutgers University in 2008. He is an assistant professor of mathematics at Oregon State University. His research interests include circle packing, discrete conformal geometry, hyperbolic geometry, geometry and quantization of Teichmüller space.

Feng Luo is a professor of mathematics at Rutgers University. His research interests include geometry and topology of low-dimensional spaces and their applications to computer science and engineering. He obtained his B.A. degree from Peking University and his Ph.D. degree from University of California, San Diego, under the supervision of Michael Freedman.

Xianfeng David Gu received his Ph.D. degree in computer science from Harvard University in 2003. He is an associate professor of computer science and the director of the 3D Scanning Laboratory in the Department of Computer Science in the State University of New York at Stony Brook. His research interests include computer graphics, vision, geometric modeling, and medical imaging. His major work includes global conformal surface parameterization in graphics, tracking and analysis of facial expression in vision, manifold splines in modeling, brain mapping and virtual colonoscopy in medical imaging, and computational conformal geometry. He won the US National Science Foundation CAREER Award in 2004, and won Joint Research Fund for Oversea Chinese Young Scholars, National Natural Science Foundation of China, in 2006. He is a member of the IEEE. He received the Morningside Gold Medal in Applied Mathematics: International Congress of Chinese Mathematicians (ICCM) 2013.